

The nuclear and Coulomb breakup of the weakly bound ${}^6\text{Li}$ with targets in the range from $A = 59$ to 208

D.R. Otomar, P. R. S. Gomes, J. Lubian
*Instituto de Física, Universidade Federal Fluminense,
Av. Litoranea s/n, Gragoatá, Niterói, R.J., 24210-340, Brazil*

L. F. Canto
Instituto de Física, Universidade Federal do Rio de Janeiro, CP 68528, Rio de Janeiro, Brazil

M. S. Hussein
*Instituto de Estudos Avançados, Universidade de São Paulo C. P. 72012,
05508-970 São Paulo-SP, Brazil, and Instituto de Física,
Universidade de São Paulo, C. P. 66318, 05314-970 São Paulo,-SP, Brazil*

We have performed CDCC calculations for the ${}^6\text{Li} + {}^{59}\text{Co}$, ${}^{144}\text{Sm}$ and ${}^{208}\text{Pb}$ systems, to investigate the dependence of the relative importance of nuclear and Coulomb breakup on the target charge (mass) at near barrier energies. The calculations were in good agreement with the experimental elastic scattering angular distributions for these systems and then, their predictions to the nuclear, Coulomb and total breakup were investigated. Although the relative importance of the nuclear breakup is, as expected, larger for lighter targets, this effect is not very pronounced. We also investigate a scaling of the nuclear breakup with the target mass and we compare the predictions for the integrated total breakup cross sections with experimental fusion cross sections at similar energies.

PACS numbers: 24.10Eq, 25.70.Bc, 25.60Gc

I. INTRODUCTION

The breakup of weakly bound nuclei has been a subject of great interest in the last years [1], both theoretically and experimentally. Among the main investigations within this field, there are studies of the breakup cross section and the influence of the breakup process on other reaction channels. The conclusions from those investigations may change with the characteristics of the weakly bound nuclei (from now on we will assume that they are the projectiles), the targets and energy regime involved. For example, halo nuclei which have extremely low breakup energy threshold may behave differently from stable weakly bound nuclei like ${}^6\text{Li}$, ${}^7\text{Li}$ and ${}^9\text{Be}$. Usually, it is assumed that Coulomb breakup predominates over nuclear breakup when heavy targets are involved. The situation may be different in the case of light targets. Thus, the nature of the breakup process should depend strongly on the target mass.

Regarding the influence of the breakup process on the fusion cross sections, at the present there is a general qualitative understanding that breakup enhances fusion at sub-barrier energies, whereas it produces some suppression above the barrier [2, 3]. Concerning the energy dependence of the optical potential in the scattering of weakly bound systems, several works show a behavior different from the one found for tightly bound systems. This behaviour is usually called the *breakup threshold anomaly* (BTA) [4]. Recently it has been shown experimentally that transfer processes followed by breakup may predominate over direct breakup of stable weakly bound nuclei

at sub-barrier energies [5–8].

In the present work we investigate the breakup process evaluating separate contributions from the Coulomb and from the nuclear fields, as well as the Coulomb-nuclear interference. We perform calculations for collisions of ${}^6\text{Li}$ projectiles with ${}^{59}\text{Co}$, ${}^{144}\text{Sm}$ and ${}^{208}\text{Pb}$, at near-barrier energies. Since the target's atomic numbers are 27, 62 and 82, one may consider ${}^6\text{Li} + {}^{59}\text{Co}$, ${}^6\text{Li} + {}^{144}\text{Sm}$ and ${}^6\text{Li} + {}^{208}\text{Pb}$ as a light system, a medium system and a heavy system, respectively. The choice of these systems was based on the availability of elastic scattering data in the literature. In this way, we could check the reliability of our calculations through comparisons with the scattering data.

The present paper is organised as follows. In section II we present the theoretical method used in the calculations. In sections III to V we show the results and discuss them. Finally, in section VI we present the conclusions of our work.

II. CDCC CALCULATIONS

It is widely accepted that the most suitable approach to deal with the breakup process, which feeds states in the continuum, is the so called continuum discretized coupled channel (CDCC) method [9, 10]. In this type of calculations, the continuum wave functions are grouped in bins or wave packets that can be treated similarly to the usual bound inelastic states, since they are described by square-integrable wave functions. In the present work

we use the same assumptions and methodology adopted in the CDCC calculations of Ref. [11], where the elastic scattering of the ${}^6\text{Li} + {}^{144}\text{Sm}$ system was investigated. We present below a summary of the main points of the CDCC method. Further details of the calculations can be found in Refs. [9–11].

Collisions involving ${}^6\text{Li}$ projectiles are influenced by the continuum states, representing mainly the breakup of ${}^6\text{Li}$ into a deuteron and an alpha particle. Owing to the low threshold of this breakup reaction ($S_\alpha = 1.47$ MeV), the breakup channel is strongly coupled with the elastic channel. Thus, it is necessary to include the continuum in the coupled channel calculation and this can be done with the CDCC method. For this purpose, we use the cluster model in which ${}^6\text{Li}$ is described as a bound state of the $d + \alpha$ system and the breakup channel is represented by the continuum states of this system. This model has been successfully used in previous CDCC calculations in collisions of ${}^6\text{Li}$ projectiles [12, 13]. The numerical calculations were performed using the computer code FRESKO [14]. In the cluster model, the projectile-nucleus interaction is written as

$$V(\mathbf{R}, \mathbf{r}, \xi) = V_{\alpha-\tau}(\mathbf{R}, \mathbf{r}, \xi) + V_{d-\tau}(\mathbf{R}, \mathbf{r}, \xi) \quad (1)$$

where \mathbf{R} is the vector joining the projectile's and target's centers, \mathbf{r} is the relative vector between the two clusters (d and α), and ξ stands for any other intrinsic coordinate describing the projectile-target system.

In our calculations, the continuum states of ${}^6\text{Li}$ are discretised as in Refs. [11, 15, 16]. Thus, we do not repeat the details here. The interaction between the d and the α clusters within ${}^6\text{Li}$ is given by a Woods-Saxon potential, with the same parameters as in Refs. [11, 15, 16].

The real parts of the $V_{\alpha-\tau}(\mathbf{R}, \mathbf{r}, \xi)$ and $V_{d-\tau}(\mathbf{R}, \mathbf{r}, \xi)$ interactions were given by the double-folding São Paulo potential [17]. We have assumed that the mass densities of the d and α clusters, required for the double-folding calculation, can be approximated by the charge densities multiplied by two, whereas the mass densities of the ${}^{59}\text{Co}$, ${}^{144}\text{Sm}$ and ${}^{208}\text{Pb}$ targets were taken from the systematic study of Ref. [17]. The imaginary parts of $V_{\alpha-\tau}(\mathbf{R}, \mathbf{r}, \xi)$ and $V_{d-\tau}(\mathbf{R}, \mathbf{r}, \xi)$ were chosen as to represent short-range fusion absorption. They were given by Woods-Saxon functions with depth $W_0 = -50$ MeV, radial parameter $r_{0i} = 1.06$ fm and diffusivity $a_i = 0.2$ fm. These imaginary potentials correspond to taking ingoing wave boundary conditions.

The present CDCC calculations include also inelastic channels, corresponding to collective excitations of the targets. These channels were selected according to the specific nuclear structure properties of the target. For ${}^{144}\text{Sm}$, the excitations included were the one-phonon quadrupole (2^+ , $E^* = 1.660$ MeV) and octupole (3^+ , $E^* = 1.8102$ MeV) first order vibrations. The values of the deformation parameters were obtained from Ref. [18] and [19] for the quadrupole and octupole deformations, respectively. For the ${}^{208}\text{Pb}$ target, we consider collec-

tive 3^- ($E^* = 2.6145$ MeV) and 5^- ($E^* = 3.1977$ MeV) states. The deformation parameters were taken from Ref. [20]. As for the ${}^{59}\text{Co}$ target the quintuplet of identified states associated with the 2^+ collective excitations were approximated by a single level with the energy equal to the centroid of the multiplet and the deformation length corresponding to that of the combined states [21].

III. RESULTS OF THE CDCC CALCULATIONS

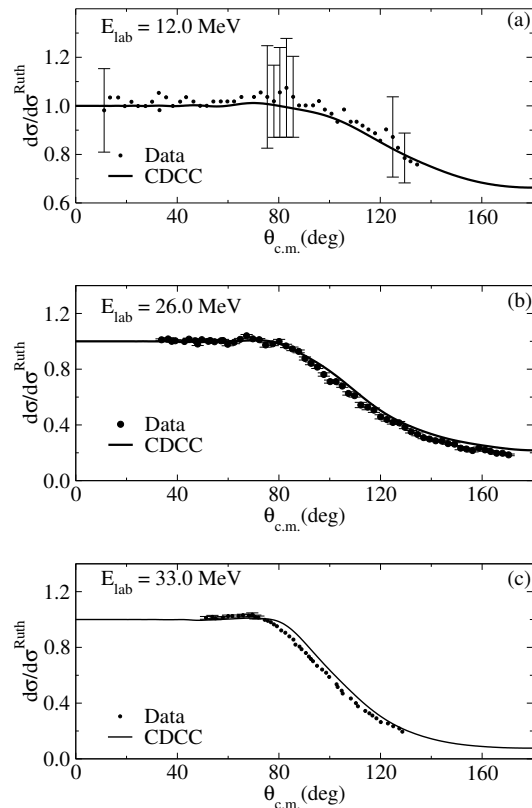


FIG. 1: Elastic scattering angular distributions for the three systems investigated. The data for the ${}^{59}\text{Co}$ (panel (a)), ${}^{144}\text{Sm}$ (panel (b)) and ${}^{208}\text{Pb}$ (panel (c)) targets are respectively from Refs. [22], [23] and [24].

In this section, we present the results of our CDCC calculations for the breakup of ${}^6\text{Li}$ projectiles, in collisions with ${}^{59}\text{Co}$, ${}^{144}\text{Sm}$ and ${}^{208}\text{Pb}$ targets. As a preliminary step, we checked that the predictions of the method for the elastic scattering of these systems were in good agreement with the available data. The situation is illustrated in figure 1, which compares theory and experiment at one near-barrier energy for each system. The good agreement obtained in the case of elastic scattering justifies the use of the model in calculations of other processes.

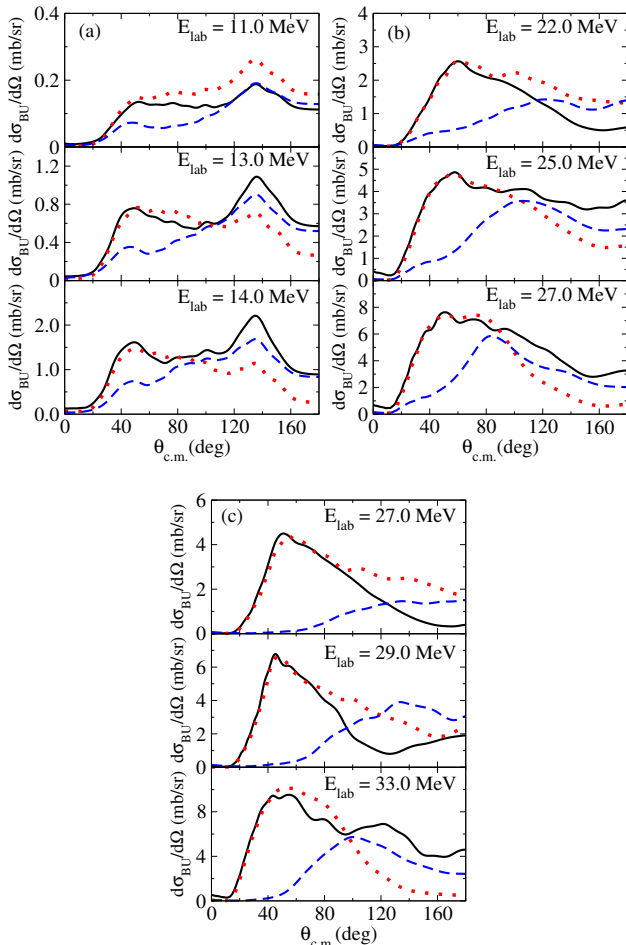


FIG. 2: (Color online) Breakup angular distributions at 3 near-barrier energies for the systems discussed in the text. In each case, we show the total breakup cross section (solid lines) together with the cross sections for pure Coulomb (short-dashed lines) and pure nuclear (long-dashed lines) breakup. As in the previous figure, panels (a), (b) and (c) correspond respectively to results for the ^{59}Co , ^{144}Sm and ^{208}Pb targets.

A. Angular distributions in ^6Li breakup

We now turn to the calculations of breakup cross sections, with the purpose of assessing the relative importance of the Coulomb and the nuclear contributions to the breakup process. We begin with a study of angular distributions. In figure 2, we show the breakup cross sections at 3 near-barrier energies for each of the systems mentioned above. The figures exhibit the total breakup cross section, together with the separate contributions from Coulomb and nuclear breakup. The systems and the collision energies are given inside each subfigure. As a reference, we mention that the heights of the Coulomb barrier calculated with the São Paulo potential are $V_B(^{59}\text{Co}) = 12.8$ MeV, $V_B(^{144}\text{Sm}) = 23.8$ MeV and $V_B(^{208}\text{Pb}) = 29.4$ MeV. Note that for each system the lowest energy in the figure is below the bar-

rier whereas the highest is above it. Inspecting figure 2, we note that at the lowest energies the Coulomb contribution tends to dominate. In fact, for energies much below the barrier one expects that only Coulomb breakup can take place, owing to the short-range of the nuclear forces. On the other hand, at energies above the barrier Coulomb breakup dominates in the breakup at forward angles whereas nuclear breakup tends to dominate at large angles. This is not surprising, since large angle scattering corresponds to small impact parameters, for which the trajectories reach small projectile-target separations, within the reach of the nuclear forces.

The transition from the Coulomb dominated angular region to the nuclear dominated one occurs at some crossing angle, θ_0 , which is a function of the collision energy. We have investigated the energy dependence of this angle for the three systems of figure 2. The results are given in figure 3, which shows the crossing angle as a function of the collision energy, normalised with respect to the barrier height. First, we notice that the crossing angle grows monotonically as the collision energy decreases. In this way, there is a critical energy below which Coulomb breakup dominates at all angles. Thus, in this energy region there is no crossing angle. The second interesting feature of this figure is that the results have a very weak dependence on the target. Thus, θ_0 can be approximated as a single function of E/V_B , even for targets in different mass ranges.

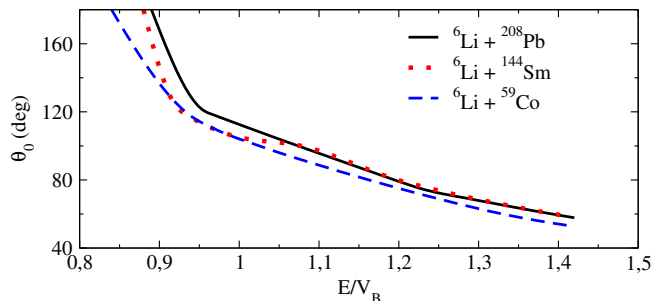


FIG. 3: (Color online) The crossing angle, θ_0 , above which nuclear breakup dominates the breakup angular distribution. For details see the text.

B. Integrated breakup cross sections

We now investigate the total breakup cross sections, integrating the angular distributions of the previous subsection over angles. Results for the systems of the previous figures at three collision energies are given in table I. The three energies for the different systems correspond to approximately the same values of $E_{c.m.}/V_B$.

Table I shows some interesting properties of the breakup cross sections. First, one notices that, as expected, the Coulomb breakup cross sections are systematically larger for heavier systems. On the other hand, the strongest nuclear breakup occurs for the intermediate

| ${}^6\text{Li} + {}^{59}\text{Co}$ | | | | |
|-------------------------------------|-----------------------------------|-----------------------------------|-----------------------------------|---|
| E_{lab} | $\sigma_{\text{Nuc}}^{\text{BU}}$ | $\sigma_{\text{Cou}}^{\text{BU}}$ | $\sigma_{\text{tot}}^{\text{BU}}$ | $(\sigma_{\text{tot}}^{\text{BU}} - \sigma_{\text{Nuc}}^{\text{BU}}) / \sigma_{\text{Cou}}^{\text{BU}}$ |
| 11.0 | 0.84 | 1.44 | 1.11 | 0.19 |
| 13.0 | 4.33 | 5.31 | 5.68 | 0.25 |
| 14.0 | 8.72 | 9.27 | 11.56 | 0.31 |
| ${}^6\text{Li} + {}^{144}\text{Sm}$ | | | | |
| E_{lab} | $\sigma_{\text{Nuc}}^{\text{BU}}$ | $\sigma_{\text{Cou}}^{\text{BU}}$ | $\sigma_{\text{tot}}^{\text{BU}}$ | $(\sigma_{\text{tot}}^{\text{BU}} - \sigma_{\text{Nuc}}^{\text{BU}}) / \sigma_{\text{Cou}}^{\text{BU}}$ |
| 22.0 | 11.3 | 22.1 | 18.8 | 0.34 |
| 25.0 | 30.0 | 41.6 | 48.0 | 0.43 |
| 27.0 | 43.6 | 57.3 | 69.6 | 0.45 |
| ${}^6\text{Li} + {}^{208}\text{Pb}$ | | | | |
| E_{lab} | $\sigma_{\text{Nuc}}^{\text{BU}}$ | $\sigma_{\text{Cou}}^{\text{BU}}$ | $\sigma_{\text{tot}}^{\text{BU}}$ | $(\sigma_{\text{tot}}^{\text{BU}} - \sigma_{\text{Nuc}}^{\text{BU}}) / \sigma_{\text{Cou}}^{\text{BU}}$ |
| 27.0 | 8.8 | 34.9 | 29.3 | 0.58 |
| 29.0 | 22.8 | 46.8 | 37.2 | 0.31 |
| 33.0 | 38.7 | 66.8 | 82.5 | 0.66 |

TABLE I: Integrated breakup cross section for the systems discussed in the text, for three collision energies. The energies are given in MeV and the cross sections in mb.

mass ${}^{144}\text{Sm}$ target. This is probably associated with the distance of closest approach and the width of the effective barrier in this collision but a quantitative interpretation of this behaviour would require further study. An important remark is that adding the nuclear with the Coulomb breakup cross sections, one does not get the total breakup cross section. For example, in the case of ${}^6\text{Li}$ breakup with the ${}^{208}\text{Pb}$ target at 29 MeV, the Coulomb breakup cross section alone is larger than the total breakup cross section. The same happens for the other systems at the lowest collision energy (below the barrier). This is a consequence of destructive Coulomb-nuclear interference in the breakup process. Note that this effect can also be observed in the angular distributions (e.g. figure 2 for the ${}^{208}\text{Pb}$ target at 29 MeV, around $\theta \sim 120$ degrees). The last column of table I shows the ratio $(\sigma_{\text{tot}}^{\text{BU}} - \sigma_{\text{Nuc}}^{\text{BU}}) / \sigma_{\text{Cou}}^{\text{BU}}$. Note that this ratio is always less than one. This fact clearly shows the destructive character of the nuclear-Coulomb interference.

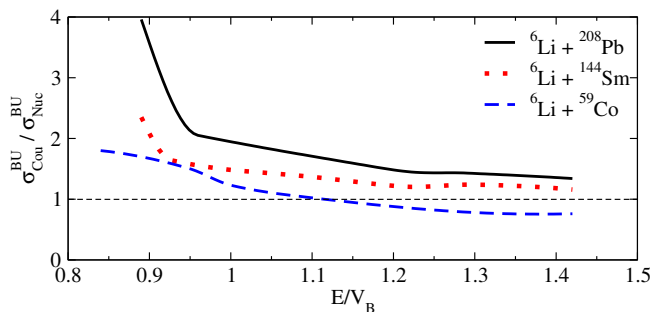


FIG. 4: (Color online) Coulomb to nuclear ratio of integrated breakup cross section for the three systems under investigation.

A more systematic study of the relative importance of the Coulomb and the nuclear forces in the breakup process is presented in figure 4, which shows the ratio $\sigma_{\text{Cou}}^{\text{BU}} / \sigma_{\text{Nuc}}^{\text{BU}}$, as a function of E/V_B . One can observe that near the Coulomb barrier this ratio is larger than unity for the three systems. However, the relative importance of the Coulomb breakup decreases as the energy increases. In the case of the lightest target, the ratio becomes smaller than one for $E/V_B > 1.1$. As expected, for the same values of E/V_B this ratio increases with the target's charge. However, the difference between the Co and Sm targets, at the same relative energies, is very small.

IV. SCALING OF THE BREAKUP CROSS SECTIONS

An interesting feature of the nuclear breakup cross section is the so-called “scaling” law, which says that this quantity at high enough energies (several tens of MeV/nucleon) should depend on the mass number of the target nucleus as [25, 26].

$$\sigma_{\text{Nuc}}^{\text{BU}} = P_1 + P_2 A_T^{1/3}, \quad (2)$$

where the parameters P_1 and P_2 depend on the projectile, the structure of the target and the bombarding energy. Ref. [26] gives results of detailed CDCC calculations of elastic scattering and breakup cross sections for halo and non-halo systems. They study collisions of ${}^8\text{B}$ (one proton-halo nucleus), ${}^{11}\text{Be}$ (one neutron-halo nucleus) and ${}^7\text{Be}$ (normal, non-halo nucleus) projectiles, from several target nuclei. It was found that the above scaling law works best for the nuclear breakup of the normal ${}^7\text{Be}$ projectile. For the halo projectiles, the scaling law works only approximately. In fact, the cross sections for these projectiles show a maximum for targets of intermediate mass, decreasing for heavy targets such as ${}^{208}\text{Pb}$.

In the present work we test the scaling law at lower energies, close to the Coulomb barrier. Plotting the nuclear breakup cross section as a function of $A_T^{1/3}$, for the same bombarding energy, as it was done for high energies, one finds that they decreases with the target mass. This is because the cross section changes rapidly as the collision energy reaches the Coulomb barrier. To eliminate this effect, we normalise the collision energy with respect to the Coulomb barrier. That is, we compare cross sections for the same value of $E_{\text{c.m.}}/V_B$.

In figure 5, we show the nuclear breakup cross sections of ${}^6\text{Li}$ as functions of $A_T^{1/3}$. The results are for $E_{\text{c.m.}}/V_B = 0.84$ (panel (a)), 1.00 (panel (b)), and 1.07 (panel (c)). The general behavior resembles the high energy results of Ref. [26], for the non-halo weakly bound ${}^7\text{Be}$ nucleus. In fact the almost straight lines that represent the curves for $E_{\text{c.m.}}/V_B = 0.84, 1.00,$ and 1.07 are fitted with $P_1 = -14.76, -62.60$ and -49.89 mb, and $P_2 = 4.11, 16.94$ and 15.41 mb, respectively. The rather large and

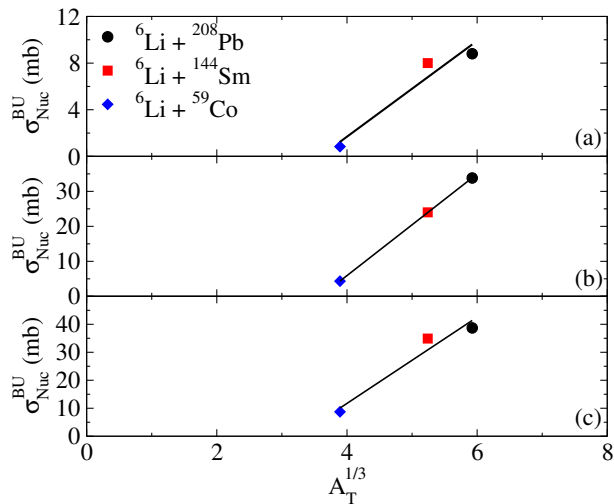


FIG. 5: (Color online) Scaling of the nuclear breakup cross sections as a function of $A_T^{1/3}$ for the systems discussed in the text, at $E_{c.m.}/V_B = 0.84$ (panel (a)), 1.00 (panel (b)) and 1.07 (panel (c)).

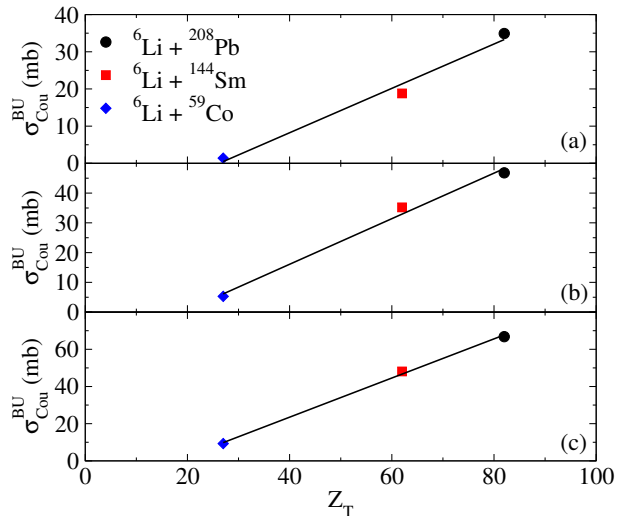


FIG. 6: (Color online) Scaling of the Coulomb breakup cross sections as a function of Z_T for the systems discussed in the text. Panels (a), (b) and (c) correspond respectively to results at $E_{c.m.}/V_B = 0.84$, 1.00 and 1.07.

negative values of P_1 are presumably traced back to barrier penetration effects, which limit the use of the geometrical picture behind the scaling law. On the other hand, at above-barrier energies the values of P_2 , which supply the slopes of the curves, are practically equal. Accordingly, the modified scaling law presented here should supply a useful and easy way to estimate the nuclear breakup cross section at other energies close to the barrier, and for other target nuclei.

One can also derive a scaling law for the Coulomb breakup cross section. In figure 6, we plot $\sigma_{\text{Cou}}^{\text{BU}}$ vs.

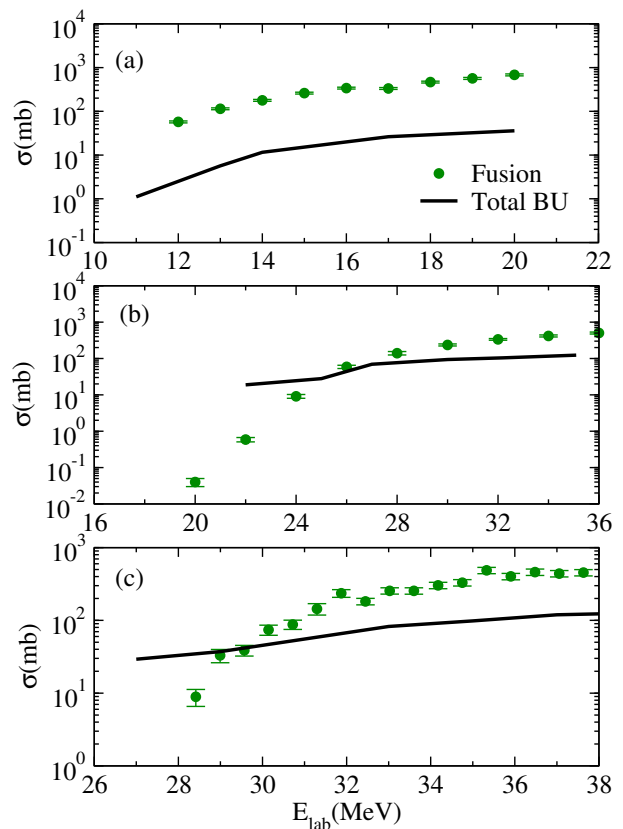


FIG. 7: (Color online) Comparisons of the fusion and the breakup cross sections for collisions of ${}^6\text{Li}$ projectiles with the ${}^{59}\text{Co}$ (panel (a)), ${}^{144}\text{Sm}$ (panel (b)) and ${}^{208}\text{Pb}$ (panel (c)) targets, at near-barrier energies.

Z_T , for the three systems discussed in the text. Panels (a), (b) and (c) correspond respectively to results for $E/V_B = 0.84, 1.00$ and 1.07 . The figures show that the Coulomb breakup cross sections depend linearly on Z_T , to a very good approximation. This behaviour can be qualitatively explained as follows. First, we point out that the electromagnetic coupling matrix-elements are proportional to Z_T , which leads to a Z_T^2 dependence in the Coulomb breakup cross section. On the other hand, the cross sections for reaction channels are proportional to a $1/E_{c.m.}$ factor [27]. Since in each panel the collision energy corresponds to the same $E_{c.m.}/V_B$ ratio, and V_B is roughly proportional to Z_T , one gets a $1/Z_T$ factor. The combination of the two arguments presented above leads to the linear dependence obtained in figure 6.

V. COMPARISON BETWEEN FUSION AND BREAKUP CROSS SECTIONS

Now we compare the predicted integrated breakup cross sections with the experimental values of the corresponding fusion cross section. We consider the same systems of the previous section, and use the fusion data

of Refs. [28–30]. Figure 7 shows these comparisons. First, one notices that the breakup cross section for the light ${}^6\text{Li} + {}^{59}\text{Co}$ system is nearly two orders of magnitude smaller than the fusion cross section. Another interesting point is that the ratio of these cross sections is roughly constant in the whole energy interval of the figure. For the medium-mass and heavy systems, ${}^6\text{Li} + {}^{144}\text{Sm}$ and ${}^6\text{Li} + {}^{208}\text{Pb}$, the situation is different. The breakup cross section is dominant at low energies whereas the fusion cross section dominates at high energies. The transition takes place in the neighbourhood of the Coulomb barrier. This behaviour is due to the Coulomb contribution to breakup. As the energy decreases below the barrier, the fusion process falls off exponentially. This is because fusion takes place when the projectile tunnels through the potential barrier. On the other hand, the decrease of Coulomb breakup is much slower. As the collision energy decreases, the classical turning point increases. Thus, the Coulomb part of the breakup coupling becomes weaker. However, the electromagnetic interactions at long distances fall as $r^{-(\lambda+1)}$ (where λ is the multipolarity of the interaction), which is much slower than the exponential fall off.

VI. CONCLUSIONS

We have investigated the nature of ${}^6\text{Li}$ breakup in near-barrier energy collisions, with targets in different mass ranges (${}^{50}\text{Co}$, ${}^{144}\text{Sm}$ and ${}^{208}\text{Pb}$). Our theoretical cross sections are based on CDCC calculations, which were shown to lead to accurate predictions of the available scattering data.

For each system, we studied the importance of contributions from the nuclear and from the Coulomb fields.

We found that at low enough energies ($E_{\text{c.m.}} < 0.9 V_{\text{B}}$), the breakup process is mainly due to Coulomb forces, for any scattering angle. In this energy region, the nuclear and the Coulomb amplitudes for the breakup process interfere destructively. In this way, the cross section for pure Coulomb breakup may be larger than the cross section arising from the simultaneous action of the Coulomb and the nuclear fields. Above the Coulomb barrier, Coulomb breakup was shown to dominate at forward angles whereas nuclear breakup is dominant at larger angles. The transition takes place at some angle θ_0 , which increases with decreasing energies. A study of the energy dependence of the transition angle indicated that it becomes nearly system independent if plotted as a function of the energy normalised with respect to the Coulomb barrier.

We have shown that the nuclear breakup cross section has a nearly linear dependence of $A_{\text{T}}^{1/3}$ as suggested in Ref. [26], for collisions at higher energies. On the other hand, the Coulomb breakup cross section was shown to depend linearly of the target charge, as could be predicted by qualitative arguments.

Finally, we made a comparison of our theoretical breakup cross sections with the available fusion data. We concluded that the latter are about two orders of magnitude larger than the former for the light ${}^6\text{Li} + {}^{50}\text{Co}$ system. For heavier systems, the breakup cross section becomes more important below the Coulomb barrier.

Acknowledgements

The authors would like to thank the financial support from CNPq, CAPES, FAPERJ, FAPESP and the PRONEX.

-
- [1] L.F. Canto, P.R.S. Gomes, R. Donangelo, M.S. Hussein, *Phys. Rep.* **424**, 1 (2006).
 - [2] L.F. Canto, P.R.S. Gomes, J. Lubian, L.C. Chamon, E. Crema; *J. Phys. G* **36**, 015109 (2009); *Nucl. Phys. A* **821**, 51 (2009).
 - [3] P. R. S. Gomes, J. Lubian, L. F. Canto, *Phys. Rev. C* **79**, 027606 (2009).
 - [4] M.S. Hussein, P. R. S. Gomes, J. Lubian, L. C. Chamon, *Phys. Rev. C* **73**, 044610 (2006).
 - [5] D. H. Luong *et al.*, *Phys. Lett. B* **695**, 105 (2011).
 - [6] M. Dasgupta *et al.*, *Nucl. Phys. A* **834**, 147c (2010).
 - [7] R. Rafiei *et al.*, *Phys. Rev. C* **81**, 024601 (2010).
 - [8] A. Shrivastava *et al.*, *Phys. Lett. B* **633**, 463 (2006).
 - [9] M. Kamimura, M. Yahiro, Y. Iseri, Y. Sakuragi, H. Kameyama, and M. Kawai, *Prog. Theor. Phys. Suppl.* **89**, 1 (1986).
 - [10] N. Austern, Y. Iseri, M. Kamimura, M. Kawai, G. Rauscher, and M. Yahiro, *Phys. Rep.* **154**, 125 (1987).
 - [11] D. R. Otomar, J. Lubian, P.R.S. Gomes, *Europ. Phys. J. A* **46**, 285 (2010).
 - [12] Y. Sakuragi, M. Yahiro, and M. Kamimura, *Prog. Theor. Phys.* **68**, 322 (1982).
 - [13] N. Keeley and K. Rusek, *Phys. Lett. B* **357**, 9 (1996).
 - [14] I. J. Thompson, *Comput. Phys. Rep.* **7**, 3 (1988).
 - [15] A. Diaz-Torres, I. J. Thompson and C. Beck, *Phys. Rev. C* **68**, 044607 (2003).
 - [16] D. R. Otomar *et al.*, *Phys. Rev. C* **80**, 034614 (2009).
 - [17] L.C. Chamon *et al.*, *Phys. Rev. Lett.* **79**, 5218 (1997); *Phys. Rev. C* **66**, 014610 (2002).
 - [18] S. Raman, C. W. Nestor, Jr., and P. Tikkanena, *At. Data, Nucl. Data Tables* **78**, 1 (2001).
 - [19] T. Kibédi and R. H. Spear, *At. Data, Nucl. Data Tables* **80**, 35 (2002).
 - [20] M.J. Martin, *Nucl. Data Sheets* **108**, 1583 (2007).
 - [21] C.M. Baglin, *Nucl. Data Sheets* **95**, 215 (2002).
 - [22] F.A. Souza *et al.*, *Phys. Rev. C* **75**, 044601 (2007).
 - [23] J.M. Figueira *et al.*, *Phys. Rev. C* **81**, 024613 (2010).
 - [24] N. Keeley *et al.* *Nucl. Phys. A* **571**, 326 (1994).
 - [25] J. C. Acquadro, M. S. Hussein, D. Pereira, and O. Sala, *Phys. Lett. B* **100**, 381(1980).
 - [26] M. S. Hussein, R. Lichtenthaler, F. M. Nunes, and I. J. Thompson, *Phys. Lett. B* **640**, 91 (2006).

- [27] C. Y. Wong, *Phy. Rev. C* **86**, 064603 (2012).
- [28] C. Beck *et al.*, *Phys. Rev. C*, **67**, 054602 (2003).
- [29] P.K. Rath *et al.*, *Phys. Rev. C*, **79**, 051601 (2009).

- [30] Y.W. Wu *et al.*, *Phys. Rev. C*, **68** 044605 (2003).